EPJ manuscript No.
(will be inserted by the editor)

Population dynamics in compressible flows

Roberto Benzi[(1)], Mogens H. Jensen[(2)],David R. Nelson[(3)] , Prasad Perlekar [(4)], Simone Pigolotti [(5)] , Federico Toschi [(4)]

[(1)] Dip. di Fisica and INFN, Università "Tor Vergata", Via della Ricerca Scientifica 1, I-00133 Roma, Italy.
[(2)]The Niels Bohr Institut, Blegdamsvej 17, DK-2100 Copenhagen, Denmark.
[(3)] Lyman Laboratory of Physics, Harvard University, Cambridge, MA 02138, USA
[(4)] Department of Physics, Department of Mathematics and Computer Science, and J.M. Burgerscentrum, Eindhoven University of Technology, 5600 MB Eindhoven, The Netherlands;
and International Collaboration for Turbulence Research.
[(5)] Dept. de Fisica i Eng. Nuclear, Universitat Politecnica de Catalunya Edif. GAIA, Rambla Sant Nebridi s/n, 08222 Terrassa, Barcelona, Spain

Abstract. Organisms often grow, migrate and compete in liquid environments, as well as on solid surfaces. However, relatively little is known about what happens when competing species are mixed and compressed by fluid turbulence. In these lectures we review our recent work on population dynamics and population genetics in compressible velocity fields of one and two dimensions. We discuss why compressible turbulence is relevant for population dynamics in the ocean and we consider cases both where the velocity field is turbulent and when it is static. Furthermore, we investigate populations in terms of a continuos density field and when the populations are treated via discrete particles. In the last case we focus on the competition and fixation of one species compared to another

1 Introduction

Challenging problems arise when spatial migrations of species are combined with population genetics. Stochastic number fluctuations are inevitable at a frontier, where the population size is small and the discrete nature of the organisms becomes essential. Depending on the parameter values, these fluctuations can produce important changes with respect to the deterministic predictions [1,2]. When two or more species undergo a Darwinian competition in a spatial environment, one must deal with additional issues such as genetic drift (stochastic fluctuations in the local fraction of one species compared to another) and Fisher genetic waves, [3] which allow more fit species to replace less fit ones. On solid surfaces, the complexities of spatial population genetics are elegantly accounted for by the stepping stone model, originally introduced by Kimura and Weiss [4], [5].

However, much of population genetics, from the distant past up to the present, played out in liquid environments, such as lakes, rivers and oceans. For example, there are fossil evidence for oceanic photosynthetic cyanobacteria (likely pre- cursors of chloroplasts in plants and a major source of oxygen in the atmosphere) that date back a billion years or more [6]. In addition, it has recently become possible to perform satellite observations of chlorophyll concentrations to identify fluid dynamical niches of phytoplankton types off the eastern coast of the southern tip of South America [7], where the domains of the species are largely determined by the tangential velocity field obtained from satellite altimetry. In cases such as these, spatial growth and evolutionary competition take place in the presence of advecting flows, some of them at high Reynolds numbers [8].

Phytoplankton needs light and nutrients to grow and many phytoplankton species are able to adjust their density and swim to stay near the surface. Nutrients are brought to the surface from deeper ocean layers, usually below 500 meters. Therefore, oceanic circulation plays an important role in shaping spatial growth and evolution of plankton species. To appreciate the complexity of the problem, it is worthwhile to shortly review our present knowledge on the basic mechanisms one should consider. In a three dimensional turbulent flow at high Reynolds number, the velocity field is fluctuating over a range of scales $[L, \eta]$ where L is the scale of energy pumping in the system and $\eta \equiv (\nu^3/\epsilon)^{1/4}$ is the Kolmogorov dissipation scale. The velocity field is also fluctuating in time. According to Kolmogorov theory, one can define the dissipation time scale as $\tau_\eta \equiv \sqrt{\nu/\epsilon}$. In the upper oceanic mixed layer , forcing is provided by heat and momentum exchange with atmosphere and the observed values [9] of ϵ ranges from $10^{-7} cm^2/sec^3$ up to $50 cm^2/sec^3$, which implies $\eta \in [0.01, 2] cm$ and $\tau_\eta \in [0.01, 300] sec$. The phytoplankton size lies in the range $[10, 200] \mu m$ with a density difference respect to sea water density in the range $[0.01, 0.1]$. Advection of individuals in the ocean should be studied by considering all forces acting on them. In particular, because of density mismatch and finite size, individuals are not advected as simple Lagrangian tracers [10] [11] , i.e. the velocity field experienced by each individual is not the Lagrangian velocity field, but an effective velocity field which may be not incompressible. A suitable measure of compressibility can be defined as $\kappa = \langle (div\ \mathbf{v})^2 \rangle / \langle (\nabla \mathbf{v})^2 \rangle$, where $\langle .. \rangle$ stands for space and time average. Using the above mentioned values of phytoplankton size a, density mismatch $\delta\rho/\rho$ and turbulent energy dissipation ϵ, one obtains

$$\sqrt{\kappa} = \frac{\delta\rho}{\rho} \frac{a^2}{\nu \tau_\eta} \in [10^{-9}, .4]$$

Another very important feature to be considered is the ability of individuals to swim in a preferential direction towards the largest concentration of nutrients (chemotaxis). The swimming velocity V_c is presently estimated in the range $[10, 500] \mu m/sec$. Because of turbulent, individuals are subject to external forces which try to change the direction. It is observed that with a characteristic time $B \sim 5 sec$, individuals try to recover the preferential direction. This mechanism, named gyrotaxis [12] and [13], introduces an effective compressible flow with compressibility

$$\sqrt{\kappa} = \frac{V_c B}{\eta} \in [2.510^{-3}, 1]$$

It is important to remark that turbulent flows with an effective compressibility can dramatically change population dynamics: concentration of individuals increases in low pressure regions (sinks) and decreases in high pressure regions (source) and the population is spatially characterized by small scale patchiness. The above discussion shows that intense turbulent activity in the oceanic upper layer may introduce non trivial effect, due to compressibility, in the phytoplankton growth and evolution at rather small scale. The same considerations might be

relevant for large scale motions. Very large scale oceanic circulation $(100 - 300 km)$ are characterized by relatively small Rossby number Ro, defined as $Ro = u_H/(fL)$, where u_H is the characteristic horizontal velocity, order $0.1 m/sec$, $f = 10^{-4} sec^{-1}$ is the Coriolis frequency and L is the characteristic large scale circulation. For $Ro << 1$, the velocity field is close to the geostrophic balance, meaning that the Coriolis force balances the pressure gradient. Under such circumstances, the vertical velocity w is rather small and it can be estimated to be $0.1 mm/sec$ or equivalently few meters/day. The horizontal velocity can be decomposed in the geostrophic component $\mathbf{v}_g$ and the non geostrophic part $\mathbf{v}_a$ where $div_H \mathbf{v}_g = 0$ and $div_H \mathbf{v}_a + \partial_z w = 0$ with $div_H \equiv \partial_x + \partial_y$. According to quasi-geostrophic dynamics, near the surface there exists an effective compressible flow acting on time scale order $div\ \mathbf{v}_a \sim 10^{-6} sec^{-1}$ much longer than the longest population growth rate $\mu \sim 2\ 10^{-5} sec^{-1}$. Therefore, at very large scale, population dynamics evolves under the advection of an incompressible flow. The above picture changes dramatically if we consider flows at Ro close to 1. Recent numerical simulations as well as direct observations [14],[15], [16] have shown that surface density tends to develop sharp horizontal gradients (fronts) especially near by the edge of oceanic eddies. Formation of intense fronts,

produced by the enhanced filamentation of surface density [17] [18], increases the vertical advection and destroy geostrophic balance. As a results two important phenomena seem to take place in the ocean at relatively large scale (order $10km$) [19][20]: regions of relative large and positive vertical velocity (upwelling) tends to increase nutrients for phytoplankton providing an increase of total biological mass while regions of negative vertical velocity increases concentration of the phytoplankton population. Frontogenesis, as it is usually named the formation of sharp density gradients, can develop vertical velocity up to few millimeter/sec. Consequently, the horizontal velocity near frontogenetic regions is characterized by an effective compressibility with $div_H \mathbf{v} \sim 10^{-4}$ [19], i.e. smaller than the population growing rate. The above picture suggests the formation of plankton patchiness on scale ranging from $100m$ to $10 - 30km$. As a tentative conclusion to our short review of phytoplankton in the ocean, albeit the complexity of the problem, it seems important to understand the role of turbulent compressible flows in population dynamics and population genetics trying to understand, at least in the simplest cases, if a new and non trivial phenomenology can be discovered and its relevance to biological evolution.

In these lectures we review our recent work [21],[22],[23] on population dynamics and population genetics in compressible velocity fields of one and two dimensions, motivated by the above discussion. We consider cases both where the velocity field is turbulent and when it is static. Furthermore, we investigate populations in terms of a continuos density field and when the populations are treated via discrete particles. In the last case we focus on the competition and fixation of one species compared to another.

2 One dimensional case

In this section we shall discuss some qualitative and quantitative ideas underlying the effect of compressible turbulence on population dynamics. We restrict ourself to the one dimensional case where most concepts can be discussed using rather simple analytical tools.

Upon specializing to one dimension, the Fisher equation reads [24]

$$\partial_t c + \partial_x (uc) = D\partial_x^2 c + \mu c - bc^2 \tag{1}$$

Equation (1) is relevant for the case of compressible flows, where $\partial_x u \neq 0$, and for the case when the field $c(x,t)$ describes the population of inertial particles or biological species. By suitable rescaling of $c(x.t)$, we can always set $b = \mu$. In the following, unless stated otherwise, we shall assume $b = \mu$ whenever $\mu \neq 0$ and $b = 0$ for $\mu = 0$.

The Fisher equation for $u = 0$ has travelling front solutions which can be computed analytically:

$$c(x,t) = \frac{1}{[1 + Cexp(-5\mu t/6 \pm x\sqrt{\mu/D}/6)]^2} \tag{2}$$

From (2) we can see that the non linear wave propagates with velocity $v_F \sim (D\mu)^{1/2}$ [3], [24]. In Fig. (1) we show a numerical solution of Eq. (1) with $D = 0.005$, $\mu = 1$ and $u = 0$ obtained by numerical integration on a space domain of size $L = 1$ with periodic boundary conditions. The figure shows the space-time behaviour of $c(x,t)$ for $c(x,t) = 0.1, 0.3.0, 5.0, 7$ and 0.9. With initial condition $c(x, t = 0)$ nonzero on only a few grid points centered at $x = L/2$, $c(x,t)$ spreads with a velocity $v_F \sim 0.07$ and, after a time $L/v_F \sim 4$ reaches the boundary. Note that the characteristic size of the Fisher'wave interface thichness is order $\sqrt{D/\mu}$.

Let us consider first the case $\mu = b = 0$. In this limit, Eq. (1) is just the Fokker-Planck equation describing the probability distribution $P(x,t) \equiv c(x,t)$ to find a particle in the range $(x, x + dx)$ at time t, whose dynamics is given by the stochastic differential equation:

$$\frac{dx}{dt} = u(x,t) + \sqrt{2D}\eta(t) \tag{3}$$

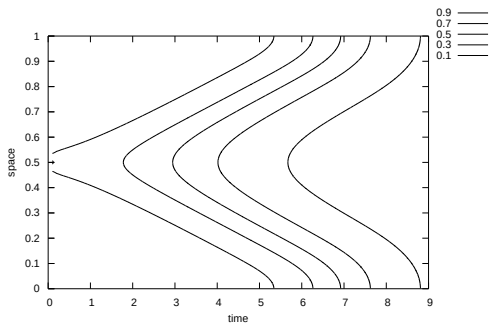

Fig. 1. Contour plot of the numerical simulation of eq. 1 with $\mu = 1$, $D = 0.005$ and with periodic boundary conditions. The initial conditions are $c(x,t) = 0$ everywhere expect for few grid points near $L/2 = 0.5$ where $c = 1$. The horizontal axis represents time while the vertical axis is space.

where $\eta(t)$ is a white noise with $\langle \eta(t)\eta(t') \rangle = \delta(t - t')$. Let us assume for the moment that $u(x,t) = u(x)$ is time independent and, moreover, let us take $u(x,t) = -\Gamma(x - x_0)$. Then, the stationary solution of (1) is given by

$$P(x,t) = A^{-1} exp[-\Gamma(x - x_0)^2/2D] \tag{4}$$

where A is a normalization constant. $P(x,t) = P(x)$ is strongly peaked near the points x_0 and (4) tells us that P spreads around x_0 with a characteristic length of order $\xi \equiv \sqrt{D/\Gamma_0}$. Hereafter, we shall refer to ξ as "quasi-localization length".

The same argument can be used to study the effect for a more generic turbulent like one dimensional field $u(x)$, still time independent. We can identify Γ as a typical gradient of the turbulent velocity field u. In a turbulent flow, the velocity field is correlated over spatial scale of order v_*/Γ where $v_*^2/2$ is the average kinetic energy of the flow. For P to be localized near a generic sink at the point x_0, despite spatial variation in the turbulent field, we must require that the localization length ξ should be smaller than the turbulent correlation scale v_*/Γ, i.e.

$$\sqrt{\frac{D}{\Gamma}} < \frac{v_*}{\Gamma} \rightarrow \frac{v_*^2}{D\Gamma} > 2 \tag{5}$$

Condition (5) can be easily understood by considering the simple case of a periodic velocity field u, i.e. $u = v_* sin(x v_*/\Gamma)$. In this case, condition (5) states that D should be small enough for the probability P not to spread over all the minima of u. For small D or equivalently for large v_*^2/Γ, the solution will be localized near the minima of u, at least for the case of a frozen turbulent velocity field $u(x)$.

The above analysis can be extended for velocity field $u(x,t)$ that depend on both space and time. The crucial observation is that, close to the sinks x_i of $u(x,t)$, we should have $u(x_i,t) \sim 0$. Thus, although u is a time dependent function, sharp peaks in $P(x,t)$ move quite slowly, simply because $u(x,t) \sim 0$ near the maximum of $P(x,t)$. One can consider a Lagrangian path $x(t)$ such that $x(0) = x_0$, where x_0 is one particular point where $u(x_0,0) = 0$ and $\partial_x u(x,0)|_{x=x_0} < 0$. From direct numerical simulation of Lagrangian particles in fully developed turbulence, we know that the acceleration of Lagrangian particles is a strongly intermittent quantitiy, i.e. it is small most of the time with large (intermittent) bursts. Thus, we expect that the localized solution of P follows $x(t)$ for quite long times except for intermittent bursts in the turbulent flow. During such bursts, the position where $u = 0$ changes abruptly, i.e. almost discontinuosly from one point, say $x(t)$, to another point $x(t+\delta t)$. During the short time interval δt, P will drift and spread, eventually reforming to become localized again near $x(t+\delta t)$. The above discussion

suggests that the probability $P(x,t)$ will be localized most of the time in the Lagrangian frame, except for short time intervals δt during an intermittent burst.

From (5) we conclude that for large value of D $P(x,t)$ is spread out, while for small enough D, P should be a localized or sharply peaked function of x most of the time. An abrupt transition, or at least a sharp crossover, from extended to sharply peaked functions P, should be observed for decreasing D.

It is relatively simple to extend the above analysis for a non zero growth rate $\mu > 0$, see also [25] for a time independent flow. The requirement (5) is now only a necessary condition to observe localization in c. For $\mu > 0$ we must also require that the characteristic gradient on scale ξ must be larger than μ, i.e. the effect of the small scale turbulent fluctuations should act on a time scale smaller than $1/\mu$. We estimate the gradient on scale ξ as $\delta v(\xi)/\xi$, where $\delta v(\xi)$ is the characteristic velocity difference on scale ξ. We invoke the Kolmogorov theory, and set $\delta v(\xi) = v_*(\xi/L)^{1/3}$ to obtain:

$$\mu < \frac{\delta v(\xi)}{\xi} = \frac{v_* \xi^{-2/3}}{L^{1/3}} = v_*(\frac{\Gamma}{LD})^{1/3} \tag{6}$$

In (6), we interpret Γ as the characteristic velocity gradient of the turbulent flow. Note also that $\delta v(\xi)/\xi \leq \Gamma$ on the average, which leads to the inequality:

$$\mu < \Gamma \tag{7}$$

From (5) and (7) we also find

$$\frac{v_*^2}{D\mu} > 2 \tag{8}$$

a second necessary condition.

One may wonder whether a non zero growth rate μ can change our previous conclusions about the temporal behavior, and in particular about its effect on the dynamics of the Lagrangian points where $u(x,t) = 0$. Consider the solution of (1) at time t, allow for a spatial domain of size L, and introduce the average position

$$x_m \equiv \int_0^L dx x \frac{c(x,t)}{Z(t)} \tag{9}$$

where $Z(t) = \int_0^L dx c(x,t)$. Upon assuming for simplicity a single localized solution, we can think of x_m just as the position where most of the bacterial concentration $c(x,t)$ is localized. We can compute the time derivative $v_m(t) = dx_m/dt$. After a short computation, we obtain:

$$v_m(t) = Z \int_0^L dx (x_m - x) P(x,t)^2 + \int_0^L u(x,t) P(x,t) dx \tag{10}$$

where $P(x,t) \equiv c(x,t)/Z(t)$. Note that v_m is independent of μ. Moreover, when c is localized near x_m, both terms on the r.h.s. of (10) are close to zero. Thus, v_m can be significantly different from zero only if c is no longer localized and the first integral on the r.h.s becomes relevant. We can now understand the effect of the non linear term in (1): when $c(x,t)$ is localized, the non linear term does not affect the value of v_m simply because v_m is close to 0. On the other hand, when $c(x,t)$ is extended the non linear term drives the system to the state $c = 1$ which is an exact solution in the absence of turbulent convection $u(x,t) = 0$.

We now discuss whether our previous analysis can be compared against numerical simulations of (1) in the one dimensional case. To completely specify equation (1) we must define the dynamics of the "turbulent" velocity field $u(x,t)$. Although we consider a one dimensional case, we want to study the statistical properties of $c(x,t)$ subjected to turbulent fluctuations

which are close to those generated by the three dimensional Navier-Stokes equations. Hence, the statistical properties of $u(x,t)$ should be characterized by intermittency both in space and in time. Although intermittency is not a crucial point in our investigations, we want to use a one dimensional velocity field with some generic features in terms of space and time dynamics. For this reason, we build the turbulent field $u(x,t)$ by appealing to a simplified shell model of fluid turbulence [26]. The wavenumber space is divided into shells of scale $k_n = 2^{n-1}k_0$, $n = 1, 2, ...$ For each shell with characteristic wavenumber k_n, we describe turbulence by using the complex Fourier-like variable $u_n(t)$, satisfing the following equation of motion:

$$(\frac{d}{dt} + \nu k_n^2)u_n = i(k_{n+1}u_{n+1}^* u_{n+2} - \delta k_n u_{n-1}^* u_{n+1} + (1-\delta)k_{n-1}u_{n-1}u_{n-2}) + f_n \ . \tag{11}$$

The model contains one free parameter, δ, and it conserves two quadratic invariants (when the force and the dissipation terms are absent) for all values of δ. The first is the total energy $\sum_n |u_n|^2$ and the second is $\sum_n (-1)^n k_n^\alpha |u_n|^2$, where $\alpha = \log_2(1-\delta)$. In this note we fix $\delta = -0.4$. For this value of δ the model reproduces intermittency features of the real three dimensional Navier Stokes equation with surprising good accuracy [26]. Using u_n, we can build the real one dimensional velocity field $u(x,t)$ as follows:

$$u(x,t) = F\sum_n [u_n e^{ik_n x} + u_n^* e^{-ik_n x}], \tag{12}$$

where F is a free parameter to tune the strength of velocity fluctuations (given by u_n) relative to other parameters in the model (see next section). In all numerical simulations we use a forcing function $f_n = (\epsilon(1+i)/u_1^*)\delta_{n,1}$, i.e. energy is supplied only to the largest scale corresponding to $n = 1$. With this choice, the input power in the shell model is simply given by $1/2\sum_n [u_n^* f_n + u_n f_n^*] = \epsilon$, i.e. it is constant in time. To solve Eqs. (1) and (11) we use a finite difference scheme with periodic boundary conditions. Theses model equations can be studied in detail without major computational efforts. The free parameters of the model are the diffusion constant D, the size of the periodic 1d spatial domain L, the growth rate μ, the viscosity ν (which fixes the Reynolds number Re), the "strength' of the turbulence F and finally the power input in the shell model, namely ϵ. Note that according to the Kolmogorov theory [27], $\epsilon \sim u_{rms}^3/L$ where u_{rms}^2 is the mean square velocity. Since $u_{rms} \sim F$, we obtain that F and ϵ are related as $\epsilon \sim F^3$. By rescaling of space, we can always put $L = 1$. We fix $\epsilon = 0.04$ and $\nu = 10^{-6}$, corresponding to an equivalent $Re = u_{rms}L/\nu \sim 3 \times 10^5$. Most of our numerical results are independent of Re when Re is large enough. In the limit $Re \to \infty$, the statistical properties of eq. (1) depend on the remaining free parameters, D, μ and F. For future reference, we compare the characteristic time scales for this simple model of homogeneous isotropic turbulence with the local doubling times of microorganisms described by Eqs. (1). Upon assuming the usual Kolmogorov scaling picture, we expect fluid mixing time scales t in the range $\nu^{1/2}/\epsilon^{1/2} < t < L^{2/3}/\epsilon^{1/3}$, or $0.01 < t < 3.0$, for typical parameter values of the shell model given above. On the other hand, the characteristic doubling time t_2 of, say, bacteria, in our model is $t_2 \sim 1/\mu$. Our simulations typically take $\mu = 1$ so that $0.2 \leq t_2 \leq 1.0$, implying cell division times somewhere in the *m*iddle of the Kolmogorov range. Microorganisms that grow *r*apidly compared to a range of turbulent mixing times out to the Kolmogorov outer scale, as is the case here, are crucial to the interesting effects we find when $\mu > 0$. Bacteria or yeast, often mechanically shaken at frequencies of order 1Hz in a test tube in standard laboratory protocols, have cell division times of 20-90 minutes, and do not satisfy this criterion. However, conditions that approximately match our simulations can be found for, say, bacterioplankton in the upper layer of the ocean, where large eddy turnover times do exceed microorganism doubling times [28], [29].

In agreement with our previous theoretical analysis, in figure (9) we show the numerical solutions of Eq. (1) for a relatively "strong" turbulent flow. A striking result is displayed: we see no trace of a propagating front: instead, a well-localized pattern of $c(x,t)$ forms and stays more or less in a stationary position. For us, Fig. (2) shows a counter intuitive result. One naive expectation might be that turbulence enhances mixing. The mixing effect due to turbulence is

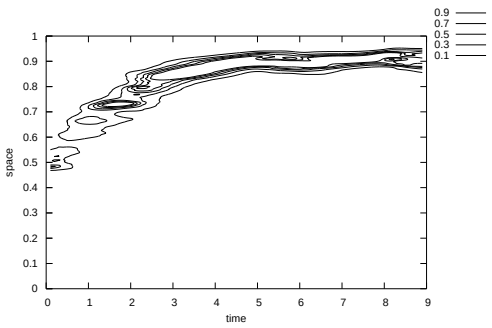

Fig. 2. Same parameters and initial condition as in Fig. (1) for equation (1) with a "strong turbulent" flow u advecting $c(x,t)$.

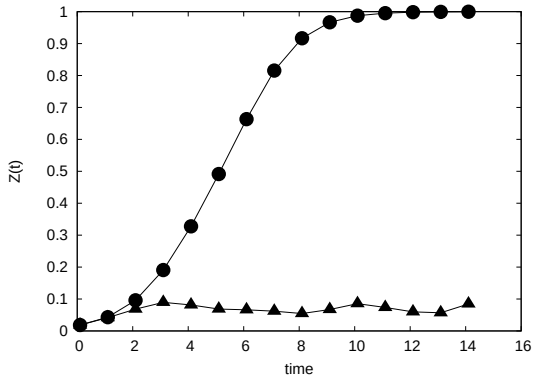

Fig. 3. The behavior in time of the total "mass" $Z(t) \equiv \int dx c(x,t)$: circles show the function Z for the case of Fig. (1), i.e. a Fisher wave with no turbulence; triangles show Z for the case of Fig. (2) when a strong turbulent flows is advecting $c(x,t)$

usually parametrized in the literature [27] by assuming an effective (eddy) diffusion coefficient $D_{eff} \gg D$. As a consequence, one naive guess for Eq. (1) is that the spreading of an initial population is qualitatively similar to the travelling Fisher wave with a more diffuse interface of width $\sqrt{D_{eff}/\mu}$ As we have seen, this naive prediction is wrong for strong enough turbulence: the solution of equation (1) shows remarkable localized features which are preserved on time scales longer than the characteristic growth time $1/\mu$ or even the Fisher wave propagation time L/v_F. An important consequence of the localization effect is that the global "mass" (of growing microorganisms, say) , $Z \equiv \int dx c(x,t)$, behaves differently with and without turbulence. In Fig. (3), we show $Z(t)$: the curve with circles refers to the conditions shown in Fig. (1)), while the curve with triangles to Fig. (2).

The behavior of Z for the Fisher equation without turbulence is a familiar S-shaped curve that reaches the maximum $Z = 1$ on a time scale L/v_F. On the other hand, the effect of turbulence (because of localization) on the Fisher equation dynamics reduces significantly Z almost by one order of magnitude

With biological applications in mind, it is important to determine conditions such that the spatial distribution of microbial organisms and the carrying capacity of the medium are significantly altered by convective turbulence. Within the framework of the Fisher equation, localization effect has been studied for a constant convection velocity and quenched time-independent spatial dependence in the growth rate μ [30], [31], [32], [33]. In our case, localization, when it happens, is a time-dependent feature and depends on the statistical properties of the compress-

ible turbulent flows. It is worth noting that the localized "boom and bust" population cycles studied here may significantly effect "gene surfing" [34] at the edge of a growing population, i.e. by changing the probability of gene mutation and fixation in the population.

One prediction of eq.s (5) and (7) is that the limit $\mu \to 0$ should be singular. More precisely, the quantity $\langle Z(t) \rangle$ must be equal to 1 for $\mu = 0$, while our predictions based on (5) and (7) imply that $\langle Z(t) \rangle < 1$ for $\mu \neq 0$ because of "quasi localization" of the solutions. In the insert of figure (4) we show the time averaged $\langle Z(t) \rangle$, computed for different values of μ for $F = 0.5$. For large μ, $< Z > \to 1$, as predicted by our phenomenological approach, while in the limit $\mu \to 0$ the values of $< Z >$ converges to 0.1. To predict the limit $\mu \to 0$ we can assume that $c_\mu(x,t)$ for small enough μ can be obtained by the knowledge of the solution $c_0(x,t)$ at $\mu = 0$ by the relation

$$c_\mu(x,t) =^s Z_\mu c_0(x,t) \tag{13}$$

where in the above equation the symbol $=$ means "in the statistical sense" and $Z_\mu = \langle c_\mu \rangle_x$ (the subscript x indicates average on space). Since the solution $c_\mu(x,t)$ satisfies the constrain $\langle c_\mu \rangle_x - \langle c_\mu^2 \rangle_x = 0$ for any μ, we obtain:

$$Z_\mu - Z_\mu^2 \langle c_0^2 \rangle_x = 0 \quad \to \quad Z_\mu = \frac{1}{\langle c_0^2 \rangle_x} \tag{14}$$

Once again we remark that eq. (14) should be interpreted in a statistical sense, i.e. the time average of Z_μ should be equal for small μ to the time average of $\langle c_0^2 \rangle_x^{-1}$. In the insert of figure (4) the blue dotted line corresponds to the time average of $\langle c_0^2 \rangle_x^{-1}$: equation (14) is clearly confirmed by our numerical findings. As we shall see in the next section, the same argument can be applied for two dimensional compressible flow.

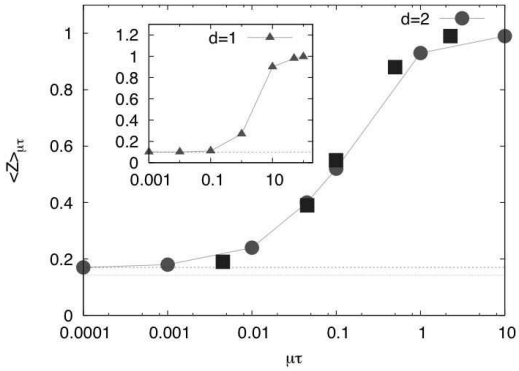

Fig. 4. Behavior of the carrying capacity $\langle Z \rangle_\mu$ as a function of $\mu\tau$ from 128^2 (dots) and 512^2 (squares) numerical simulations with $Sc = 1$. Note that for $\mu\tau \to 0.001$, the carrying capacity approaches the limit $1/\langle P^2 \rangle$ (dotted line) predicted by Eq. (21). In the inset we show similar results for one dimensional compressible turbulent flows.

3 Fisher equation in two dimensional compressible flows

As discussed in the previous section, an advecting compressible turbulent flow leads to highly non-trivial dynamics for the Fisher equation. Although previous results were obtained only in one dimension using a synthetic advecting flow from a shell mdel of turbulence, two striking effects were observed: the concentration field $c(\boldsymbol{x},t)$ is strongly localized near transient but long-lived sinks of the turbulent flows for small enough growth rate μ; in the same limit, the space-time average concentration (denoted in the following as carrying capacity) becomes much

smaller than its maximum value 1. Here, we present numerical results aimed at understanding the behavior of the Fisher'equation for two dimensional compressible turbulent flows and extending our previous results to more realistic two dimensional turbulent flows. Our model consists in assuming that the microorganism concentration field $c(\boldsymbol{x}, t)$, whose dynamics is described by the equation

$$\partial_t c + \nabla \cdot (\mathbf{u}c) = D\nabla^2 c + \mu c(1-c) \tag{15}$$

We assume that the population is constrained on a planar surface of constant height in a three dimensional fully developed turbulent flow with periodic boundary conditions. Such a system could be a rough approximation to microorganisms that actively control their bouyancy to mantain a fixed depth below the surface of a turbulent fluid. As a consequence of this choice, the flow field in the two dimensional slice becomes compressible [38]. We consider here a turbulent advecting field $\mathbf{u}(\mathbf{x}, t)$ described by the Navier-Stokes equations, and nondimensionalize time by the Kolmogorov time-scale $\tau \equiv (\nu/\epsilon)^{1/2}$ and space by the Kolmogorov length-scale $\eta \equiv (\nu^3/\epsilon)^{1/4}$. The non-dimensional numbers charecterizing the evolution of the scalar field $C(\mathbf{x}, t)$ are then the Schmidt number $Sc = \nu/D$ and the non-dimensional time $\mu\tau$. A particularly interesting regime arises when the doubling time μ^{-1} is somewhere in the middle of the range of eddy turnover times that characterize the turbulence. Although the underlying turbulent energy cascade is somewhat different [42], this situation arises for oceanic plankton, who double in ~ 12 hours, in a medium with eddy turnover times varying from minutes to months [43].

We conducted a three dimensional direct numerical simulation (DNS) of homogeneous, isotropic turbulence at two different resolutions (128^3 and 512^3 collocation points) in a cubic box of length $L = 2\pi$. The Taylor microscale Reynolds number [27] for the full 3D simulation was $Re_\lambda = 75$ and 180, respectively, the viscosities were $\nu = 0.01$ and $\nu = 2.05 \cdot 10^{-3}$, the total energy dissipation rate was around $\epsilon \simeq 1$ in both cases. For the analysis of the Fisher equation we focused only on the time evolution of a particular 2D slab taken out of the full three dimensional velocity field and evolved a concentration field $c(\boldsymbol{x}, t)$ constrained to lie on this plane only. A typical plot of the $2d$ concentration field, along with the corresponding velocity divergence field (taken at time $t = 86$, $Re_\lambda = 180$) in the plane is shown in Fig. 5 ($Sc = 5.12$): the concentration $c(x, y, t)$ is highly peaked in small areas, resembling one dimensional filaments. When the microorganisms grow faster than the turnover times of a significant fraction of the turbulent eddies, $c(\mathbf{x}, t)$ grows in a quasi-static compressible velocity field, and accumulates near sinks and along slowly contracting eigendirections, leading to filaments. The geometry of the concentration field suggests that $c(\mathbf{x}, \mathbf{t})$ is different from zero on a set of fractal dimension d_F much smaller than 2. A box counting analysis of the fractal dimension of $c(\mathbf{x}, \mathbf{t})$ supports this view and provides evidence that $d_F = 1. \pm 0.15$.

Note that for $\mu = 0$, Eq. (15) reduces to the Fokker-Planck equation describing the probability distribution $P(x, y, t)$ to find a Lagrangian particle subject to a force field $\mathbf{u}(\mathbf{x}, t)$ at x, y at time t:

$$\frac{\partial P}{\partial t} + \boldsymbol{\nabla} \cdot (\boldsymbol{u}P) = D\nabla^2 P \tag{16}$$

The statistical properties of P have been studied in several works (e.g. [39] and [40]) and it is known that for compressible turbulence $P(\mathbf{x}, t)$ exhibits a nontrivial multifractal scaling. Upon multiplying eqn. (16) by P and integrating in space we obtain: $\frac{1}{2}\partial_t \left\langle P^2 \right\rangle_s + \frac{1}{2} \left\langle P^2(\nabla \cdot \mathbf{u}) \right\rangle_s = -D \left\langle (\nabla P)^2 \right\rangle_s$ where $\langle \dots \rangle_s$ denotes a spatial integration. In the statistically stationary regime, the above equation reduces to:

$$\frac{1}{2}\langle P^2(\nabla \cdot \mathbf{u}) \rangle = -D\langle (\nabla P)^2 \rangle, \tag{17}$$

where now $\langle \dots \rangle$ stands for space and time average. Eq. (17) shows that for $\nabla \cdot \mathbf{u} = 0$ the only possible solution is $P = const.$ However, compressibility leads to nontrivial dynamics such that P^2 and $\nabla \cdot \mathbf{u}$ are anticorrelated. We measure the degree of compressibility by the factor $\kappa \equiv \langle (\nabla \cdot \mathbf{u})^2 \rangle / \langle (\nabla \mathbf{u})^2 \rangle$, and estimate the l.h.s. of Eq. (17) by assuming $\langle P^2(\nabla \cdot \mathbf{u}) \rangle =$

$-A_1\langle P^2\rangle\langle(\nabla\cdot\mathbf{u})^2\rangle^{1/2}$, where we used the so called one point closure for turbulent flows [27] and A_1 is expected to be order unity. We estimate the r.h.s of Eq. (17) by assuming:

$$\langle(\nabla P)^2\rangle = A_2\frac{\langle P^2\rangle}{\xi^2} \tag{18}$$

where we define ξ the "quasi-localization" length of P, which is expected to be of the same order of the width of the narrow filaments in Fig. 5. Finally we set $\langle(\nabla\mathbf{u})^2\rangle = \epsilon/\nu$ where ϵ is the mean rate of energy dissipation and ν is the viscosity. On putting everything together we find a localization length given by:

$$\xi^2 = \frac{2A_2D\sqrt{\nu}}{A_1\sqrt{\kappa\epsilon}}. \tag{19}$$

One important quantity -from the biological point of view- is the carrying capacity,

$$Z(t) = \frac{1}{L^2}\int dxdyc(\boldsymbol{x};t), \tag{20}$$

and in particular its time average in the statistical steady state with growth rate μ, $\langle Z(t)\rangle_\mu$. We are interested to understand how $\langle Z\rangle_\mu$ behaves as a function of μ, in the two important limits $\mu\to\infty$ and $\mu\to 0$. In the limit $\mu\to\infty$, we expect the carrying capacity attains its maximum value $\langle Z\rangle_{\mu\to\infty} = 1$, because when the characteristic time $1/\mu$ becomes much smaller than the Kolmogorov dissipation time $\tau_\eta \equiv (\nu/\varepsilon)^{1/2}$, the effect of the velocity field is a relatively small perturbation on the rapid growth of the microorganisms. Indeed, consider a perturbation expansion of $c(\mathbf{x},t)$ in terms of $\delta = 1/\mu$. On defining $c \equiv \sum_i \delta^i c_i(\mathbf{x},t)$, substituting in Eq. (15), assuming steady state, and collecting the terms up to $\mathcal{O}(\delta^2)$ we find $c \approx 1-\epsilon(\boldsymbol{\nabla}\cdot\boldsymbol{u}) + \epsilon^2\{\boldsymbol{\nabla}\cdot[\boldsymbol{u}(\boldsymbol{\nabla}\cdot\boldsymbol{u})] - D\nabla^2(\nabla\cdot\boldsymbol{u}) - (\boldsymbol{\nabla}\cdot\boldsymbol{u})^2\} + \mathcal{O}(\delta^3)$. The above analysis shows that in the limit $\mu\to\infty$ the concentration field tends to become uniform with the leading correction coming from the local compressibility. After substituting the expansion of c in Eq. (20) one gets $Z \approx 1-(\delta^2/L)\int(\boldsymbol{\nabla}\cdot\boldsymbol{u})^2\mathrm{dx} + \mathcal{O}(\delta^3)$. Note that the leading correction to the carrying capacity is of order δ^2, is consistent with the physical picture presented above.

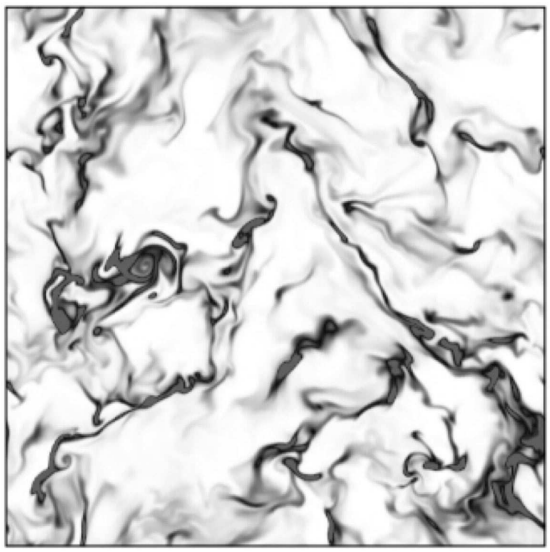

Fig. 5. Plot of the concentration $c(x,y,t)$. The white color indicate regions with low concentration while regions of high concentration are denoted by black.

By defining $\Gamma \equiv \langle (\boldsymbol{\nabla} \cdot \boldsymbol{u})^2 \rangle^{1/2}$ as the r.m.s value of the velocity divergence, we expect a crossover in the behavior of $\langle Z \rangle_\mu$ for $\mu < \Gamma$. In the limit $\mu \to 0$, following our discussion in the previous section, we expect that:

$$\lim_{\mu \to 0} \langle Z \rangle_\mu = \frac{1}{\langle P^2 \rangle}. \tag{21}$$

We have tested both Eq.(21) and the limit $\mu \to \infty$ against our numerical simulations. In Fig. (4) we show the behavior of $\langle Z \rangle_\mu$ for the numerical simulations discussed in this section. The horizontal line represents the value $1/\langle P^2 \rangle$ obtained by solving Eq. (16) for the same velocity field and $\mu = 0$. For our numerical simulations we estimate $\Gamma = 4.0$ and we observe, for $\mu > \Gamma$ the carrying capacity $\langle Z \rangle_\mu$ becomes close to its maximum value 1. The limit $\mu \to 0$ requires some care. Let us define $\tau_b \equiv 1/\mu$ to be the time scale for the bacteria to grow. The effect of turbulence is relevant for τ_b longer than the Kolmogorov dissipation time scale τ_η. We also expect that τ_b must be smaller than the large scale correlation time $\tau_L \sim (L^2/\epsilon)^{1/3}$, which depends on the forcing mechanism driving the turbulent flows and the large scale L. Thus, the limit $\mu \to 0$ can be investigated either for $L \to \infty$ or by forcing the system with a constant energy input which slows down the large scale, as it is the case in our numerical simulations

The limit $\mu \to 0$ can be investigated more accurately as follows: according to known results on Lagrangian particles in compressible turbulent flows, we know that P should have a multifractal structure in the inviscid limit $\nu \to 0$ [11]. If our assumption leading to Eq. (21) is correct, $c(\mathbf{x}, t)$ must show multifractal behavior in the same limit with multifractal exponents similar to those of P. For analytical results, see Ref. [39] . Numerical evidence for the multifractal behavior of Lagrangian tracers in compressible flows can be found in Ref. [38].

We perform a multifractal analysis of the concentration field $c(x, y, t)$ with $\mu > 0$ by considering the average quantity $\tilde{c}_\mu(r) \equiv \frac{1}{r^2} \int_{B(r)} c(x, y, t) dx dy$ where $B(r)$ is a square box of size r. Then the quantities $\langle \tilde{c}_\mu(r)^p \rangle$ are expected to be scaling functions of r, i.e. $\langle \tilde{c}_\mu(r)^p \rangle \sim r^{a(p)}$, where $a(p)$ is a non linear function of p with $a(2) = -0.47$, see [22] for details.

Our multifractal analysis allow us to investigate the possible relation between the localization length ξ defined in Eq. (18) and the carrying capacity $\langle Z \rangle_\mu$. The localization length ξ can be considered as the smallest scale below which one should observe fluctuations of $c(x, t)$. Thus we can expect that $\langle P^2(x, t) \rangle \sim \xi^{a(2)}$. Using (21) we obtain $\langle Z \rangle \sim \xi^{-a(2)}$. In the inset of Figure (6) we show $\langle Z \rangle$ as a function of ξ (obtained by using (18) for $\mu = 0.01$ and different values of the diffusivitiy D. According to Eq. (19), reducing the diffusivity D will shrink the localization length ξ and hence $\langle Z \rangle_\mu$. From Figure (6) a clear power law behavior is observed with a scaling exponent 0.46 very close to the predicted behavior $-a(2) = 0.47$.

Finally, we discuss bacterial populations subject to both turbulence and uniform drift because of, e.g., sedimentation under the action of gravity field. In this case, we can decompose the velocity field into zero mean turbulence fluctuations plus a constant "wind" velocity u_0. In presence of a mean drift velocity Eq. 15 becomes:

$$\frac{\partial c}{\partial t} + \boldsymbol{\nabla} \cdot [(\boldsymbol{u} + u_0 \hat{e_x}) c] = D \nabla^2 c + \mu c (1 - c) \tag{22}$$

where $\hat{e_x}$ is the unit vector along the x-direction. Note that the mean drift breaks the Galilean invariance as the concentration c is advected by the wind, while turbulent fluctuations $\mathbf{u}$ remain fixed. In Fig. 6 we show the variation of carrying capacity versus u_0 for two different values of μ and fixed diffusivity $D = 0.015$. We find that for $u_0 \leq u_{rms}$ (u_{rms} is the root-mean-square turbulent velocity) the carrying capacity Z saturates to a value equal to the value of Z in absence of u_0 i.e., quasilocalization by compressible turbulence dominate the dynamics. For $u_0 > u_{rms}$ the drift velocity delocalizes the bacterial density thereby causing $Z \to 1$, in agreement with the results discussed in [37].

4 Discrete population dynamics

The population dynamics of a single species expanding into new territory was first studied in the pioneering works of Fisher, Kolmogorov, Petrovsky and Piscounov (FKPP) [3,24,1]. Later,

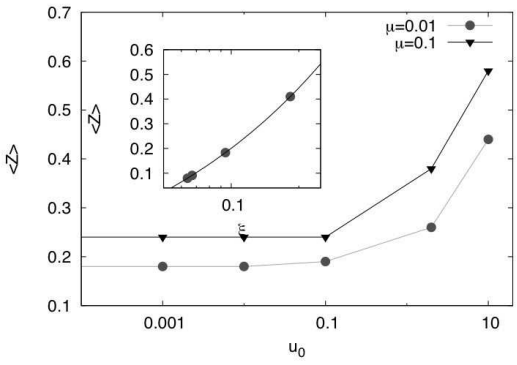

Fig. 6. Main figure: plot of $\langle Z \rangle$ as function of a super imposed external velocity u_0 for $\mu = 0.01$ (bullets) and $\mu = 0.1$ (triangles). Inset: log-log plot of $\langle Z \rangle$ as a function of the localization length ξ defined in Eq. (18) for $u_0 = 0$. The slope is consistent with the prediction $< Z > \sim \xi^{-a(2)}$ discussed in the text. The numerical simulations are done for $\mu = 0.01$ and different values of D from $D = 0.05$ to $D = 0.001$.

Kimura and Weiss studied individual-based counterparts of the FKPP equation [4], revealing the important role of number fluctuations. In particular, stochasticity is inevitable at a frontier, where the population size is small and the discrete nature of the individuals becomes essential. Depending on the parameter values, fluctuations can produce radical changes with respect to the deterministic predictions [1,2]. If $f(x,t)$ is the population fraction of, say, a mutant species and $1 - f(x,t)$ that of the wild type, the stochastic FKPP equation reads in one dimension [5]:

$$\partial_t f(x,t) = D\partial_x^2 f + sf(1-f) + \sqrt{D_g f(1-f)}\xi(x,t) \tag{23}$$

where D is the spatial diffusion constant, D_g is the genetic diffusion constant (inversely proportional to the local population size), s is the genetic advantage of the mutant and $\xi = \xi(x,t)$ is a Gaussian noise, delta-correlated in time and space that must be interpreted using Ito calculus [5]. In the neutral case ($s = 0$), number fluctuations induce a striking effect in the population dynamics, namely segregation of the two species. One can show that the dynamics of competing species in 1D can be characterized by the dynamics of boundaries between the $f = 0$ and $f = 1$ states of Eq. 23, which perform a random walk. This effect is theoretically predicted by Eq.(23) and confirmed experimentally in the linear inoculation experiments on neutral variants of fluorescently labelled bacteria illustrated in Fig. (8a) [41].

We study the influence of advection on the dynamics of two distinct populations consisting of discrete 'particles'. Due to competition and stochasticity, interactions between two populations usually drive one of the two populations to extinction. The average time of this event (the *f*ixation time) is a quantity of great biological interest since it determines the amount of genetic and ecological diversity that the system can sustain. Studying competition in a hydrodynamics context, where both a compressible velocity field and stochasticity due to finite population sizes are present, calls for a nontrivial generalization of Eq. (23). One complication is that, because of compressibility, the sum of the concentrations of the two species is no longer invariant during the dynamics.

We have overcome these problems through a off-lattice particle model designed to explore how compressible velocity fields affect biological competition. Let us consider two different organisms, A and B, which advect and diffuse in space while undergoing duplication (i.e. cell division) and density-dependent annihilation (death), see Fig. 7. Specifically, we implement the following stochastic reactions: each particle of species $i = A, B$ duplicates with rate μ_i and annihilates with a rate $\bar{\mu}_i \widehat{n}_i$, where $\widehat{n}_i$ is the number of neighboring particles (of both types) in an interaction range δ. Let N be the total number of organisms that can be accomodated in the unit interval with total density $c_A + c_B = 1$. To reduce the number of parameters, we fix $\delta = 1/N$

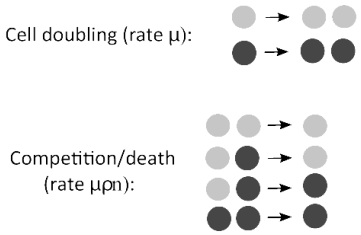

Fig. 7. The possible six birth and death processes in the particle model consisting of two species, A (red) and B (green).

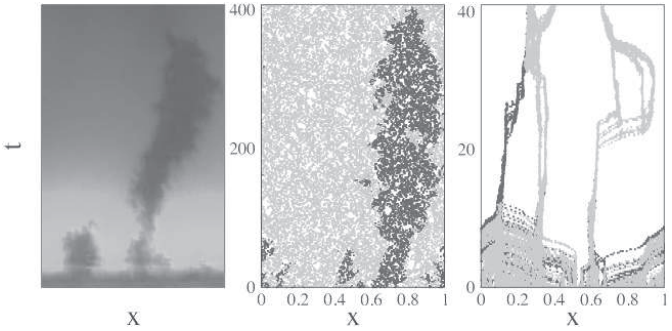

Fig. 8. (a) Experimental range expansion of the two neutra E. coli strains used in Ref. [41], but run about one day longer (D. Nelson, unpublished). The black bar at the bottom is due a small crack in the agar substrate. (b) Space-time plot of the off-lattice particle model with no advecting velocity field. A realization characterized by a pattern similar to the experimental one has been selected for illustrative purposes. (c) Particle model with a compressible turbulent velocity field. Simulations are run until fixation (disappearance of one of the two species); note the reduced carrying capacity and the much faster fixation time in (c). Parameters: $N = 10^3$, $D = 10^{-4}$, $\mu = 1$. Parameters of the shell model are as in [21].

as the average particle spacing in the absence of flow. Further, we set $\bar{\mu}_A = \bar{\mu}_B = \mu_B = \mu$, but take $\mu_A = \mu(1 + s)$ to allow for a selective advantage (faster reproduction rate) of species A. We will start by analyzing in depth the neutral case $s = 0$ and consider the effect of $s > 0$ in the end of the Letter. In one dimension and with these choices of parameters, our macroscopic coupled equations for the densities $c_A(x, t)$ and $c_B(x, t)$ of individuals of type A and B in an advecting field $v(x, t)$ read

$$\begin{aligned}\partial_t c_A &= -\partial_x(vc_A) + D\partial_x^2 c_A + \mu c_A(1+s-c_A-c_B) + \sigma_A\xi \\ \partial_t c_B &= -\partial_x(vc_B) + D\partial_x^2 c_B + \mu c_B(1-c_A-c_B) + \sigma_B\xi'\end{aligned} \tag{24}$$

with $\sigma_A = \sqrt{\mu c_A(1 + s + c_A + c_B)/N}$ and $\sigma_B = \sqrt{\mu c_B(1 + c_A + c_B)/N}$. $\xi(x, t)$ and $\xi'(x, t)$ are independent delta-correlated noise sources with an Ito-calculus interpretation as in Eq. (23).

Simulations of the particle model corresponding to (24) with $v = s = 0$ result in a dynamics similar to the one observed in experiments, as shown in Fig.(8b). In this simple limit, our model can be considered as a grand canonical generalization of Eq (23), where the total density of individuals $c_A + c_B$ is now allowed to fluctuate around an average value 1. We fix the following

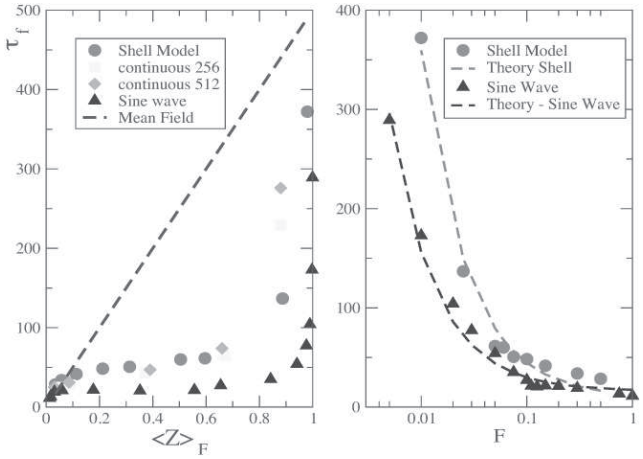

Fig. 9. Average fixation time τ_f for neutral competitions in compressible turbulence and sine wave advection, as a function of (left) the reduced carrying capacity $\langle Z\rangle_F$ and (right) forcing intensity F (small $\langle Z\rangle_F$ in the left panel corresponds to large forcing in the right panel). (left) Red circles and blue triangles are particle simulations. Other symbols denote simulations of the continuum equations with different resolutions on the unit interval. The black dashed line is the mean field prediction, $\tau_f = N\langle Z\rangle_F/2$. In (right), only particle simulations are shown and dashed lines are the theoretical prediction $\tau_f = \tau_0 + c/F$ based on boundary domains, with fitted parameters $\tau_0 = 9.5$, $c = 3.5$ in the case of the shell model and $\tau_0 = 16$, $c = 1.4$ in the case of the sine wave.

parameters: $N = 10^3$, $D = 10^{-4}$, $\mu = 1$ and $L = 1$ where L is a one dimensional domain endowed with periodic boundary conditions. With these parameters, the fixation time τ_f would be $\sim 10^4$ for the one dimensional FKKP equation, and $\sim 10^3$ for the well-mixed case.

Introducing a compressible velocity field $v(x,t)$, via the shell model 11 as shown in Fig.(8c), leads to radically different dynamics. Individuals tend to concentrate at long-lived sinks in the velocity field. Further, extinction is enhanced and the total number of individuals $n(t)$ present at time t is on average smaller than N.

In order to study how a velocity field changes τ_f, we first analyze two different velocity fields: The first is a velocity field $v(x,t)$ generated by a shell model (Eqs. 11) of compressible turbulence [21], reproducing the power spectrum of high Reynolds number turbulence with forcing intensity F. The second is a static sine wave, $v(x) = F\sin(2\pi x)$, representing a simpler case in which only one Fourier mode is present, and thus a single sink, in the advecting field. In both cases, periodic boundary conditions on the unit interval are implemented.

Fig.(9) shows the average fixation time τ_f for $s = 0$ in the first two cases, while varying the intensity F of advection. In the left panel, we plot the fixation times as a function of the time-averaged reduced carrying capacity $\langle Z\rangle_F$, where $Z(t) = n(t)/N$ is the carrying capacity reduction, i.e. the ratio between the actual number of particles and the average number of particles N observed in absence of the velocity field. Plotting vs. $\langle Z\rangle_F$ allows comparisons with the mean field prediction, $\tau_f = 2N\langle Z\rangle_F/\mu$, valid for well mixed systems (black dashed line) [5]. For the shell model, we include simulations of the macroscopic equations (24) with different resolutions (256 and 512 lattice sites on the unit interval), obtaining always similar results for τ_f vs. $\langle Z\rangle_F$.

In all cases, the presence of a spatially varying velocity field leads to a dramatic reduction of τ_f, compared to mean field theory. The fixation time drops abruptly as soon as $\langle Z\rangle < 1$, even for very small F.

Acknowledgment

We acknowledge computational support from CASPUR (Roma, Italy uner HPC Grant 2009 N. 310), from CINECA (Bologna, Italy) and SARA (Amsterdam, The Netherlands). Support for D.R.N. was provided in part by the National Science Foundation through Grant DMR-0654191

and by the Harvard Materials Research Science and Engineering Center through NSF Grant DMR-0820484. Data from this study are publicly available in unprocessed raw format from the iCFDdatabase (http://cfd.cineca.it). M.H.J. was supported by Danish National Research Foundation through "Center for Models of Life".

References

1. W. van Saarloos, Phys. Rep. **386**, 29-222 (2003).
2. O. Hallatschek and K. Korolev, Phys. Rev. Lett. **103**, 108103 (2009), and references therein.
3. R. Fisher, Ann. Eugenics **7**, 335 (1937); A. Kolmogorov, I. Petrovsky and N. Psicounoff, Moscow, Univ. Bull. Math, **1**, 1, (1937).
4. M. Kimura and G. H. Weiss, Genetics **49**, 561-576 (1964); J. F. Crow and M. Kimura An Introduction to Population Genetics, Blackburn Press, Caldwell, NJ (2009).
5. For a recent review, see K. Korolev et al. Rev. Mod. Phys. **820**, 1691-1718 (2010).
6. B. A. Whitton and M. Potts The Ecology of Cyanobacteria: Their Diversity in Time and Space eds. Kluwer, Dordrecht, Netherland
7. F. D'Ovidio et al., Proc. Natl. Acad. Sci. **107**, 18366-18370 (2010). ds (2000).
8. W. J. McKiver and Z. Neufeld, Phys. Rev. E **79**, 061902 1-8 (2009).
9. F. Peters, C. Marraese, Marine Ecology Progress Series, **205**, 291, (2000)
10. F. Toschi, E. Bodenschatz, Annual Rev. Fluid. Mech., **41**, 375, (2008)
11. J. Bec, Phys. Fluids **15**, L81-L84 (2003).
12. W. M. Durham, E. Ciment, R. Stocker, Phys. Rev. Lett., **106**, 238102, (2011)
13. C. Torney, Z. Neufeld, Phys. Rev. Lett., **99**, 078101,(2007)
14. P. Klein and G. Lapeyre, Annual Review of Marine Science, **1**, 357, (2009)
15. K. Mizobota, Saitoh SI, Shiomoto A., Miyamura T, Shiga N, et. al , Prog. Oceanogr., **55** , 65, (2002)
16. A. P. Martin, Progr. Ocean. **57**, 125-174 (2003).
17. I. M. Held, R. T. Pierrehumber, S.T. Garner, K.L. Swanson, J. Fluid. Mech., **282**, 1, (1995)
18. X. Capet, P. Klein, B.L. Hua, G. Lapeyre, J. C. McWilliams, J. Fluid. Mech., **604**, 165, (2008)
19. P. Klein, B. L. Hua, G. Lapeyre, X. Capet, S. Le Gentil, H. Sasaki, J. Phys. Oceanogr. **38**, 1748, (2008)
20. L. Thomas, A. Tandon, A. Mahadevan, J. Geophys. Res., **177**, 17, (2008)
21. R. Benzi, D. R. Nelson Physica D **238** 2003-2015 (2009).
22. P. Perlekar, R. Benzi, D.R. Nelson, Phys. Rev. Lett. **105**, 144501 (2010).
23. S. Pigolotti, R. Benzi, M.H. Jensen, D. R. Nelson, Phys. Rev. Lett. submitted.
24. A. Kolmogorov, N. Petrovsky, and N. Piscounov, Moscow Univ. Math. Bull. **1**, 1-25 (1937).
25. S. Berti, D. Vergni, A. Vulpiani Europhys. Lett. 83, 54003 (2008)
26. L. Biferale, Annu., 2003, Rev. Fluid Mech. 35, 441.
27. U. Frisch, Turbulence the legacy of A.N. Kolmogorov (Cambridge University Press, Cambridge, 1996).
28. T. Tel et. al., Chemical and Biological Activity in Open Flows: A Dynamical Systems Approach, Phys. Reports, 413, 91, 2005
29. A. R. Robinson, Proc. R. Soc. Lond. A453, 2295 (1997); A455, 1813 (1999)
30. D. R. Nelson, and N. M. Shnerb. 1998. Non-hermitian localization and population biology. Phys. Rev. E. 58:1383.
31. K.A. Dahmen, D. R. Nelson, and N. M. Shnerb. 2000. Life and death near a windy oasis. J. Math. Biol. 41:1-23.
32. N. M. Shnerb, 2001, Extinction of a bacterial colony under forced convection in pie geometry. Phys. Rev. E 63:011906, and references therein.
33. T. Neicu, A. Pradhan, D. A. Larochelle, and A. Kudrolli. 2000. Extinction transition in bacterial colonies under forced convection. Phys. Rev. E. 62:1059 - 1062.
34. O. Hallatschek and D. R. Nelson, Theor. Popul. Biology, 73,1, 158, 2007.
35. J. R. Cressman et al., Europhys. Lett. **66**, 219-225 (2004); G. Boffetta et al., Phys. Rev. Lett. **93**, 134501 (2004).
36. J. ichi Wakita *et* al., J. Phys. Soc. Jpn. **63**, 1205 (1994).
37. R. Benzi and D. Nelson, Physica D **238**, 2003 (2009).
38. G. Boffetta, J. Davoudi, B. Eckhardt, and J. Schumacher, Phys. Rev. Lett. **93**, 134501 (2004).

39. J. Bec, Phys. Fluids **15**, L81 (2003); J. Bec, J. Fluid Mech., **528**, 255 (2005).
40. G. Falkovich, K. Gawedzki, and M. Vergassola, Rev. Mod. Phys. **73**, 914 (2001).
41. O. Hallatschek and D. Nelson, Proc. Natl. Acad. Sci **104**, 19926-19930 (2007).
42. W. McKiver and Z. Neufeld, Phys. Rev. E **79**, 061902 (2009).
43. A. Martin, Prog. in Oceanography **57**, 125 (2003).
44. A. Kurganov and E. Tadmor, J. Comp. Phys. **160**, 241 (2000).